

CuSe-based layered compound $\text{Bi}_2\text{YO}_4\text{Cu}_2\text{Se}_2$ as a quasi-two-dimensional metal

S. G. Tan,^{1,*} D. F. Shao,^{1,*} W. J. Lu,¹ B. Yuan,¹ Y. Liu,¹ J. Yang,¹ W. H. Song,¹ Hechang Lei,^{1,†} and Y. P. Sun^{1,2,3,‡}

¹*Key Laboratory of Materials Physics, Institute of Solid State Physics, Chinese Academy of Sciences, Hefei 230031, People's Republic of China*

²*High Magnetic Field Laboratory, Chinese Academy of Sciences, Hefei 230031, People's Republic of China*

³*University of Science and Technology of China, Hefei 230026, People's Republic of China*

We have investigated the physical properties of a new layered oxyselenide $\text{Bi}_2\text{YO}_4\text{Cu}_2\text{Se}_2$, which crystallizes in an unusual intergrowth structure with Cu_2Se_2 and Bi_2YO_4 layers. Electric transport measurement indicates that $\text{Bi}_2\text{YO}_4\text{Cu}_2\text{Se}_2$ behaves metallic. Thermal transport and Hall measurements show that the type of the carriers is hole-like and it may be a potential thermoelectric material at high temperatures. First principle calculations are in agreement with experimental results and show that $\text{Bi}_2\text{YO}_4\text{Cu}_2\text{Se}_2$ is a quasi-2D metal. Further theoretical investigation suggests the ground states of the $\text{Bi}_2\text{YO}_4\text{Cu}_2\text{Se}_2$ -type can be tuned by designing the blocking layers, which will enrich the physical properties of these compounds.

PACS numbers: 72.15.Eb, 81.05.Bx, 81.05.Zx, 71.15.Mb

I. INTRODUCTION

Quasi-two-dimensional (quasi-2D) oxide compounds of transition-metal elements have been studied extensively because of their exotic and superior electrical and magnetic properties, such as high-temperature superconducting cuprates,¹ manganites with colossal magnetoresistance,² and cobaltite-based thermoelectric materials,³ etc.. In contrast, oxychalcogenides, which also tend to adopt layered structure due to the different sizes and coordination requirements of oxygen and the heavier chalcogenide anions, are a relatively under-investigated class of solid-state compounds.⁴ Among known layered TMCh-based (TM = Cu, Ag; Ch = S, Se, Te) oxychalcogenides, there are mainly two structural types.⁴ One structural type is representative by the LnOTMCh series (Ln = lanthanide), which can be regard as the filled PbFCl-type structure and is isostructural to ZrSiCuAs as well as iron-based superconductors LnOFePn (Pn = As, P).^{5,6} These compounds composed of alternating Ln_2O_2 fluorite layers and TM_2Ch_2 anti-fluorite layers along c axis have been studied intensively because of their superior and novel optical and transport properties originating from TM_2Ch_2 layers.⁷⁻¹⁰ Another important structural type is representative by the oxide antimonide $\text{Sr}_2\text{Mn}_3\text{Sb}_2\text{O}_2$ ¹¹ (which may conveniently be formulated as $\text{Sr}_2\text{MnO}_2\text{Mn}_2\text{Sb}_2$) and related oxide pnictides.^{12,13} Later on, this structural type is also found in $\text{Sr}_2\text{ZnO}_2\text{Cu}_2\text{S}_2$.¹⁴ In $\text{Sr}_2\text{ZnO}_2\text{Cu}_2\text{S}_2$, the chalcogenide layer $[\text{Cu}_2\text{S}_2]^{2-}$ is similar to that in LaOCuS whereas the $[\text{Sr}_2\text{ZnO}_2]^{2+}$ is not fluorite type but perovskite type. Several oxychalcogenides with this crystal structure have been reported.¹⁴⁻¹⁹

As listed in Table I, most of the reported CuCh-based layered compounds are semiconductors.^{19,21-23,26,27} But it is well-established²⁸ that the copper chalcogenide layers present in the oxysulfides can readily accept holes in the antibonding states at the top of a valence band that

TABLE I: Some typical CuCh-based compounds and their ground states.

| Compound | Ground state |
|---|---------------------------------|
| KCu_2Se_2 | Metallic ²⁰ |
| BaCu_2Se_2 | Semiconducting ²¹ |
| $\text{LaOCuS}(\text{Se})$ | Semiconducting ²² |
| $\text{BaFCuS}(\text{Se})$ | Semiconducting ²³ |
| $\text{BiOCuS}(\text{Se})$ | Semiconducting ²² |
| YOCuSe | Semiconducting ²⁴ |
| HgOCuSe | Metallic ²⁵ |
| $\text{Sr}_2\text{MnO}_2\text{Cu}_2\text{Se}_2$ | Semiconducting ¹⁹ |
| $\text{Sr}_3\text{Sc}_2\text{O}_5\text{Cu}_2\text{S}_2$ | Semiconducting ^{26,27} |
| $\text{Bi}_2\text{YO}_4\text{Cu}_2\text{Se}_2$ | Metallic |

is composed of well-mixed Cu-3d and S-3p orbitals, and these holes are very mobile. For example, $\text{La}_{1-x}\text{Sr}_x\text{OCuS}$ is a rare example of a transparent p -type semiconductor²⁹ in which the Cu-3d/S-3p valence band is doped with holes; the band gap insulator $\text{Sr}_2\text{ZnO}_2\text{Cu}_2\text{S}_2$ can also be doped to produce a metallic $\text{Na}_x\text{Sr}_{2-x}\text{ZnO}_2\text{Cu}_2\text{S}_2$ with p -type carriers with $x \sim 0.1$,³⁰ and there is an evidence for the very high mobility of p -type carriers in the related $\text{Sr}_3\text{Sc}_2\text{O}_5\text{Cu}_2\text{S}_2$ with Cu or Sr deficiencies.^{26,27} On the other hand, HgOCuSe ²⁵ isostructural to LaOCuS is a metal and KCu_2Se_2 ²⁰ in which La_2O_2 layer is replaced by alkali metal K also exhibit metallic behavior. Therefore, the physical properties of CuCh-based layered oxychalcogenides are not only determined by the intralayer interaction of CuCh layer alone but also by the interlayer interactions.

Recently, a new series of layered oxychalcogenides $\text{Bi}_2\text{LnO}_4\text{Cu}_2\text{Se}_2$ (Y, Gd, Sm, Nd, and La) were synthesized.³¹ The metallic behavior is stated for the compound $\text{Bi}_2\text{YO}_4\text{Cu}_2\text{Se}_2$ which is very rare in the CuCh-based oxychalcogenides. In this work, we systematically studied the magnetic property, electric

transport, heat capacity, thermoelectric properties and the electronic structure of the layered oxyseLENIDE $\text{Bi}_2\text{YO}_4\text{Cu}_2\text{Se}_2$. These results indicate the quasi-2D metallic ground state in this compound. We also found it may be a potential thermoelectric material at high temperatures. Furthermore, we systematically studied the doping effects of such system in theory. The results suggest that the ground state of the $\text{Bi}_2\text{YO}_4\text{Cu}_2\text{Se}_2$ -type compounds can be tuned by designing the blocking layers.

II. EXPERIMENT SECTION

$\text{Bi}_2\text{YO}_4\text{Cu}_2\text{Se}_2$ sample was prepared by reacting a stoichiometric mixture of Bi_2O_3 , Y_2O_3 , Y, Cu, and Se. The raw materials were mixed and ground thoroughly in an agate pestle and mortar, and then the mixtures were pressed into pellets under 12 MPa. The pellets were placed into dried alumina crucibles and sealed under vacuum ($< 10^{-4}$ Pa) in the silica tubes which had been baked in drybox for 1-2 h at 150 °C. The ampoules were heated to 830 °C with 1 °C/min and maintained at this temperature for 24 h. Finally the furnace is shut down and cools to room temperature naturally. The obtained samples were reground, pelletized, and heated for another 24 hours at 830 °C followed by furnace cooling.

The X-ray powder diffraction patterns were recorded at room temperature on a Panalytical diffractometer (X'Pert PRO MRD) with $\text{Cu-K}\alpha$ radiation and a graphite monochromator in a reflection mode. Structural refinement of powder $\text{Bi}_2\text{YO}_4\text{Cu}_2\text{Se}_2$ sample was carried out by using Rietica software.³² The average stoichiometry of a $\text{Bi}_2\text{YO}_4\text{Cu}_2\text{Se}_2$ polycrystalline was determined by examination of multiple points using an energy-dispersive X-ray spectroscopy (EDX) in a JEOL JSM-6500 scanning electron microscope. The XPS data were taken on an AXIS-Ultra instrument from Kratos using monochromatic Al $\text{K}\alpha$ radiation (225 W, 15 mA, 15 kV) and low-energy electron flooding for charge compensation. The magnetic susceptibility was measured by a superconducting quantum interference device magnetometer (Quantum Design MPMS). Electron paramagnetic resonance (EPR) spectra were recorded using an X-band Bruker EMX plus 10/12 cw spectrometer operating at 9.4 GHz equipped with an Oxford continuous flow cryostat within the temperature range of 2 ~ 300 K. The electrical resistivity, thermal transport property, specific heat and Hall measurements were measured using a Quantum Design Physical Properties Measurement System (PPMS).

Electronic structure was obtained from first-principles density functional theory (DFT) in the generalized gradient approximation (GGA) according to the Perdew-Burke-Ernzerhof.³³ The QUANTUM-ESPRESSO package³⁴ was used with ultrasoft pseudopotential from GBRV pseudopotential library.³⁵ The discussion about the Coulomb correlation of 3d electrons in

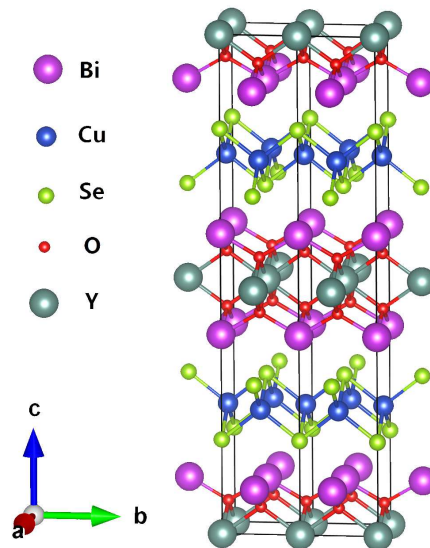


FIG. 1: The crystal structure of $\text{Bi}_2\text{YO}_4\text{Cu}_2\text{Se}_2$.

$\text{Bi}_2\text{YO}_4\text{Cu}_2\text{Se}_2$ was carried out using the GGA+ U approach in the version introduced by Anisimov *et al.*³⁶ with an approximate self-interaction correction implemented in the rotationally invariant way according to Liechtenstein *et al.*³⁷ We tested different values of the screened Coulomb parameter U . The exchange parameter J was fixed to $\sim 0.1U$. The energy cutoff for the plane-wave basis set was 40 Ry. Brillouin zone sampling is performed on the Monkhorst-Pack (MP) mesh³⁸ of $16 \times 16 \times 16$.

III. RESULTS AND DISCUSSION

A. Crystal Structure, Composition, and Valence State.

The structure of $\text{Bi}_2\text{YO}_4\text{Cu}_2\text{Se}_2$ is shown in Fig. 1, which can be described as stacking of edge-shared CuSe_4 tetrahedron layers with Bi_2YO_4 layers alternatively along c axis. Fig. 2 (a) shows the XRD pattern and the result of Rietveld refinement. The structural parameters obtained from the Rietveld refinements are listed in Tables II and III. Almost all the reflections can be indexed in the space group of $I4/mmm$. The refined lattice parameters of $\text{Bi}_2\text{YO}_4\text{Cu}_2\text{Se}_2$ are $a = 3.8628(3)$ Å and $c = 24.322(2)$ Å, which is consistent with the previous reported results for $\text{Bi}_2\text{YO}_4\text{Cu}_2\text{Se}_2$.³¹ The other weak reflections originate from the BiOCuSe impurity, and the result of the two-phase fitting reveals that the weight percentage of BiOCuSe is about 3.24%, which can be neglected to our study on $\text{Bi}_2\text{YO}_4\text{Cu}_2\text{Se}_2$. The EDX spectrum (Fig. 2 (b)) of polycrystal confirms the presence of Bi, Y, O, Cu, and Se. The average atomic ratios determined from EDX are Bi: Y: Cu: Se = 1.99(4) : 1.00(2) : 1.99(1) :

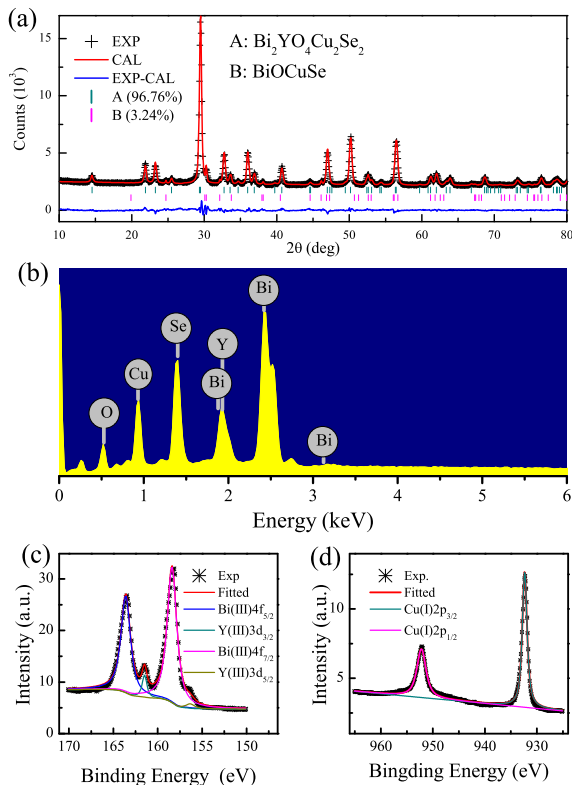


FIG. 2: (a) Result of Rietveld refinement against powder XRD diffraction data for $\text{Bi}_2\text{YO}_4\text{Cu}_2\text{Se}_2$; (b) is the EDX spectrum of the sample; (c) and (d) are the XPS spectra of Bi, Y and Cu.

1.81(5) when setting the content of Y as 1. It is consistent with the formula of $\text{Bi}_2\text{YO}_4\text{Cu}_2\text{Se}_2$ except a small amount of Se deficiency, which may be caused by the easily volatilization of Se. In order to determine the valence state of Cu, Bi, and Y, the XPS spectrum was measured for the $\text{Bi}_2\text{YO}_4\text{Cu}_2\text{Se}_2$. There are four peaks located at binding energies (BEs) of 163.6, 161.5, 158.4, and 156.4 eV, which can be attributed to Bi- $4f_{5/2}$, Y- $3d_{3/2}$, Bi- $4f_{7/2}$, and Y- $3d_{5/2}$ respectively, indicating the Bi and Y ions adopt the valence of +3.^{39,40} The monovalence state of Cu ion was reported in other CuCh-based compounds.¹⁹ As shown in Fig. 2(d), the peak position of Cu- $2p_{3/2}$ is 932.24 eV. In copper oxides, the binding energies of Cu^+ (Cu_2O) and Cu^{2+} (CuO) are 932.6 eV and 933.6 eV respectively.⁴¹ However, in copper selenides, the binding energies of Cu^+ (Cu_2Se) and Cu^{2+} (CuSe) are 931.9 eV and 932 eV respectively.⁴² Thus, it is difficult to determine the valence of Cu in $\text{Bi}_2\text{YO}_4\text{Cu}_2\text{Se}_2$ just through the measurement of XPS. Because the valences of Bi and Y are +3 and the valences of Se and O are -2 in this compound, the valence of Cu should be +1.5, i.e., a mixed valence state of $\text{Cu}^{2+}/\text{Cu}^{1+}$. A $3d^{9.5}$ configuration of Cu ion in $\text{Bi}_2\text{YO}_4\text{Cu}_2\text{Se}_2$ can be expected. The existence of partial Cu^{2+} was verified by the measurement of EPR, which will be discussed below.

TABLE II: Fractional atomic coordinates of $\text{Bi}_2\text{YO}_4\text{Cu}_2\text{Se}_2$ and BiOCuSe determined by two-phase refinement of X-ray data.

| Atom | x | y | z |
|--|-------|-------|-----------|
| $\text{Bi}_2\text{YO}_4\text{Cu}_2\text{Se}_2$ (wt%: 96.76%) | | | |
| Bi | 0.5 | 0.5 | 0.8968(1) |
| Y | 0.5 | 0.5 | 0.5 |
| O | 0 | 0.5 | 0.9353(7) |
| Cu | 0 | 0.5 | 0.25 |
| Se | 0.5 | 0.5 | 0.3110(2) |
| BiOCuSe (wt%: 3.24%) | | | |
| Bi | 0.25 | 0.25 | 0.141(2) |
| Cu | -0.25 | 0.25 | 0.5 |
| Se | -0.25 | -0.25 | 0.342(5) |
| O | -0.25 | 0.25 | 0 |

TABLE III: Structural parameters obtained from Rietveld analysis at room temperature.

| | $\text{Bi}_2\text{YO}_4\text{Cu}_2\text{Se}_2$ | BiOCuSe |
|------------------------|--|----------------------|
| space group | I4/mmm | P4/nmm |
| a (Å) | 3.8628(3) | 3.9311(7) |
| c (Å) | 24.322(2) | 8.899(3) |
| bond length | | |
| $d_{\text{Bi-O}}$ (Å) | 2.399(1) | 2.34(3) |
| $d_{\text{Bi-Se}}$ (Å) | 3.437(4) | 3.30(1) |
| $d_{\text{Cu-Se}}$ (Å) | 2.435(3) | 2.42(2) |
| bond angle | | |
| O-Bi-O | $79.02(3) \times 4$ | $73.06(1) \times 4$ |
| | $128.27(3) \times 2$ | |
| O-Y-O | $66.48(3) \times 4$ | |
| | $101.7(4) \times 2$ | |
| Se-Cu-Se | $104.94(1) \times 2$ | $108.75(1) \times 2$ |
| | $111.78(1) \times 4$ | $109.84(2) \times 4$ |

B. Physical Properties.

Figure 3 (a) shows the temperature dependence of the magnetic susceptibility of $\text{Bi}_2\text{YO}_4\text{Cu}_2\text{Se}_2$. Since the magnetic signal of the sample is too weak to be distinguished from the signal of background using the routine measurement, we took a two-step measurement: Firstly, we measured the signal of the background, and then the total signal of background and sample was measured. After subtracting the signal of the background from the raw data, a paramagnetic (PM)-like temperature dependence of susceptibility was observed with no evidence of magnetic ordering at low temperatures due to the monotonous increase in the magnetic susceptibility. Since EPR is helpful for understanding magnetic interactions and spin correlation on a microscopic level, we performed the EPR measurements. Figure 3(b) shows the EPR spectra dP/dH of $\text{Bi}_2\text{YO}_4\text{Cu}_2\text{Se}_2$ at 2, 10, 30,

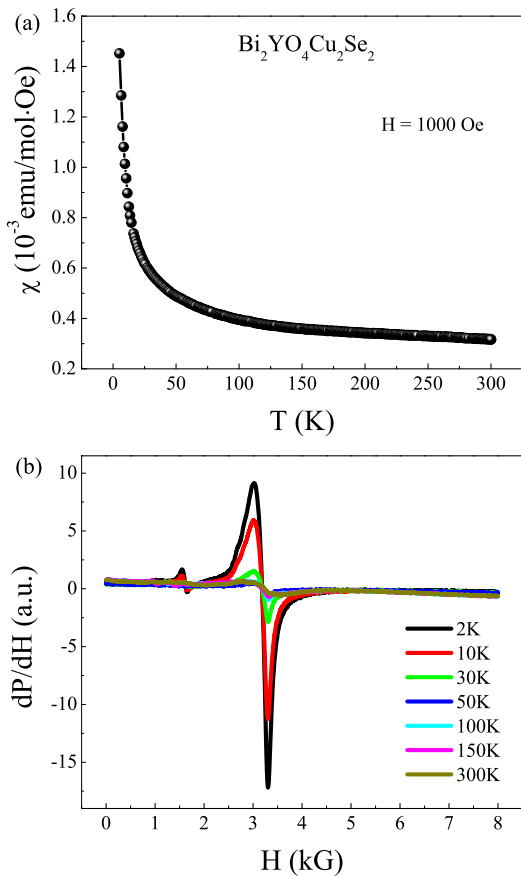


FIG. 3: (a) The temperature dependence of magnetic susceptibility $\chi(T)$ curve from 5 to 300K. (b) the EPR spectra of $\text{Bi}_2\text{YO}_4\text{Cu}_2\text{Se}_2$ at different temperatures.

50, 100, 150, and 300 K. There are two resonance lines centered at ~ 3200 Gauss and ~ 1600 Gauss, respectively. And both resonance fields are independent of temperature implying the lack of spin fluctuation. The Cu(I) ions ($3d^{10}$) should be EPR-inactive due to the lack of unpaired electrons. Therefore, the PM resonance signal at 3200 Gauss corresponding to the free-electron g factor $g_e = 2$ is attributed to the existence of Cu^{2+} ions, which is in agreement with the XPS results. Moreover, the weak resonance signal at 1600 Gauss is often concomitant with the PM resonance signal at 3200 Gauss in the Cu-contained compounds and is termed as half-field transition arising from the formation of a triplet state Cu(II) dimers.⁴³ As a result, the existence of magnetic ordering and/or spin fluctuation in $\text{Bi}_2\text{YO}_4\text{Cu}_2\text{Se}_2$ can be ruled out based on the present magnetic and EPR results.

As shown in Fig. 4, the resistivity $\rho(T)$ of polycrystalline $\text{Bi}_2\text{YO}_4\text{Cu}_2\text{Se}_2$ shows a metallic behavior in the measured temperature region. The resistance drops linearly with temperature from 300 to 100 K and the room temperature value of resistivity is $0.59 \text{ m}\Omega\cdot\text{cm}$, which is much smaller than the reported value.³¹ The temperature coefficient of resistivity is $1.7 \times 10^{-3} \text{ m}\Omega\cdot\text{cm}/\text{K}$. It

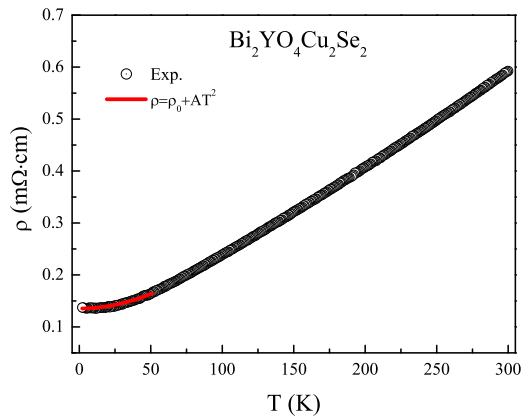


FIG. 4: Electrical resistivity of $\text{Bi}_2\text{YO}_4\text{Cu}_2\text{Se}_2$ is plotted as a function of temperature from 300 to 2 K, and the red line is the Fermi liquid fitting of the resistivity at low temperature.

should be noted that the polycrystalline BiOCuSe shows semiconducting behavior. The impurity may have some minor influence on the absolute value of resistivity, but the metallic behavior should be intrinsic. As can be seen, below 45 K the resistivity is satisfied with the equation

$$\rho(T) = \rho_0 + AT^2, \quad (1)$$

which is suggestive of Fermi liquid behavior in the ground state. The residual resistivity ρ_0 and parameter A are found to be $134.7(3) \mu\Omega \cdot \text{cm}$ and $0.01118(3) \mu\Omega \cdot \text{cm}/\text{K}^2$ respectively. The metallic behavior is consistent with our theoretical calculation results as shown below.

On the other hand, previous theoretical reports have indicated that the undoped BiOCuSe is a semiconductor and the metallic behavior of BiOCuSe is caused by Cu deficiencies which introduce holes to the system.^{22,44} In undoped BiOCuSe , the “electricity storage” layer Bi_2O_2 provides two electrons to the “conductive” layer Cu_2Se_2 . However, in $\text{Bi}_2\text{YO}_4\text{Cu}_2\text{Se}_2$, the “charge reservoir” layer Bi_2YO_4 provides only one electron to the “conductive” layer Cu_2Se_2 . Therefore, the replacement of Bi_2O_2 by Bi_2YO_4 should introduce one hole and as a result, $\text{Bi}_2\text{YO}_4\text{Cu}_2\text{Se}_2$ is a metal with p -type carriers. There will be further discussion in the calculation part.

Figure 5 shows the specific heat of $\text{Bi}_2\text{YO}_4\text{Cu}_2\text{Se}_2$ measured from 280 K to 5 K. The specific heat of $\text{Bi}_2\text{YO}_4\text{Cu}_2\text{Se}_2$ approaches to the value of $3NR$ at 280 K, where N is the atomic number in the chemical formula ($N = 11$) and R is the gas constant ($R = 8.314 \text{ J}/\text{mol}\cdot\text{K}$), consistent with the Dulong-Petit law. The inset shows the low-temperature specific heat data, $C_p(T)/T$ plotted as a function of T^2 . It can be fitted using

$$C_p = \gamma T + \beta T^3 + \delta T^5, \quad (2)$$

where γT is the electronic contribution with γ the Sommerfeld coefficient, and $\beta T^3 + \delta T^5$, originate from the lattice contribution. The fitted values of γ , β , and δ are equal to $3.6(8) \text{ mJ}/\text{mol}\cdot\text{K}$, $1.56(3) \text{ mJ}/\text{mol}\cdot\text{K}^4$, and

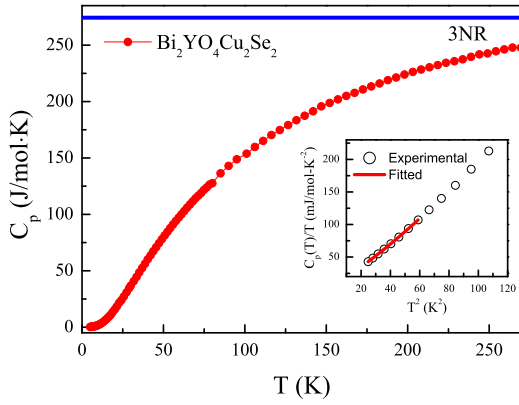


FIG. 5: Temperature dependence of specific heat for $\text{Bi}_2\text{YO}_4\text{Cu}_2\text{Se}_2$. The inset is the low temperature data $C_p(T)/T$ plotted as a function of T^2 .

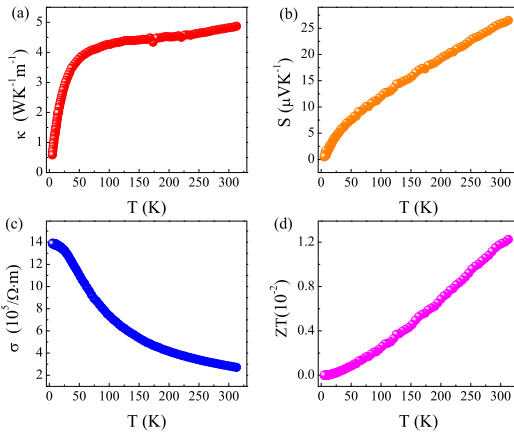


FIG. 6: (a) The thermal conductivity κ , (b) Seebeck coefficient S , (c) electrical conductivity σ and (d) figure of merit ZT as a function of temperature from 330 to 5 K.

0.0038(3) mJ/mol·K⁶ respectively. Using the formula

$$\Theta_D = \left(\frac{n \times 1.944 \times 10^6}{\beta} \right)^{1/3}, \quad (3)$$

where n is the number of atoms in a unit cell, we derived the Debye temperature $\Theta_D = 239$ K. According to the Sommerfeld theory of metals, γ can be written as function of the density of states (DOS) at Fermi level as:

$$\gamma = \frac{\pi^2 k_B^2}{3} N(E_F)(1 + \lambda), \quad (4)$$

where $N(E_F)$ is the DOS at the Fermi level and λ is the electron-phonon coupling constant. Assuming λ is 0, the obtained value of $N(E_F)$ is 1.5 states/eV/f. u..

The thermal transport measurement results including the Seebeck coefficient S , electrical conductivity σ , and thermal conductivity κ are shown in Fig. 6. The S is positive in the whole measurement temperature region, indicating the major carriers are holes. The $S(T)$ is

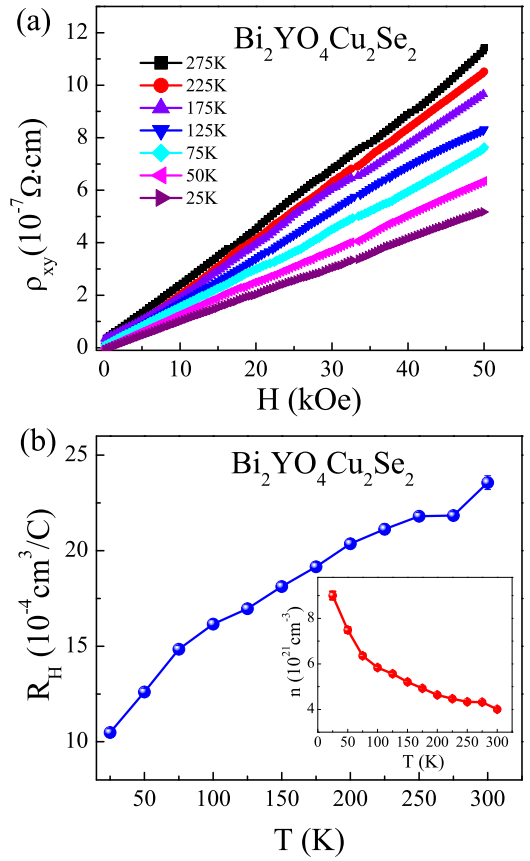


FIG. 7: (a) Field dependence of $\rho_{xy}(H)$ at various temperatures. (b) Temperature dependence of the Hall coefficient R_H of $\text{Bi}_2\text{YO}_4\text{Cu}_2\text{Se}_2$. Inset: temperature dependence of the carrier density $n = 1/|eR_H|$ calculated from R_H .

nearly linearly dependent with temperature and drops to zero at low temperature. The $\kappa(T)$ is almost constant when T is above 100 K, below which the $\kappa(T)$ drops fast near to zero. The dimensionless figure of merit, ZT ($ZT = S^2 T \sigma / \kappa$), which represents for the efficiency of a thermoelectric material, was calculated and presented in Fig. 6 (d). Due to the low resistivity, and relatively small thermal conductivity, the ZT value of our sample at 300 K reaches about 0.012. And the value of ZT increases smoothly from 5 K to 300 K. It implies $\text{Bi}_2\text{YO}_4\text{Cu}_2\text{Se}_2$ may be a potential thermoelectric material at high temperatures.

In order to confirm the type of carrier and determine the carrier density in $\text{Bi}_2\text{YO}_4\text{Cu}_2\text{Se}_2$, the magnetic field dependence of the Hall resistivity at various temperatures was measured. (Figure 7 (a)) The transverse resistivity $\rho_{xy}(H)$ is positive at all measured temperatures, indicating that the hole-type carrier is dominant, consistent with the sign of $S(T)$. The Hall coefficient $R_H = \rho_{xy}(H)/H$ at different temperatures is shown in Fig. 7 (b). It can be seen that R_H decreases with temperature. The change can be ascribed to the multiband effect, which has been observed in classic two-band superconducting

TABLE IV: The optimized lattice parameters and atomic coordinates compared with experimental values.

| | Exp. | Opt. |
|-----------------|-----------|---------|
| $a(\text{\AA})$ | 3.8628(3) | 3.888 |
| $c(\text{\AA})$ | 24.322(2) | 24.872 |
| $z(\text{Bi})$ | 0.8968(1) | 0.89895 |
| $z(\text{Y})$ | 0.5 | 0.5 |
| $z(\text{O})$ | 0.9353(7) | 0.94445 |
| $z(\text{Cu})$ | 0.25 | 0.25 |
| $z(\text{Se})$ | 0.3110(2) | 0.31106 |

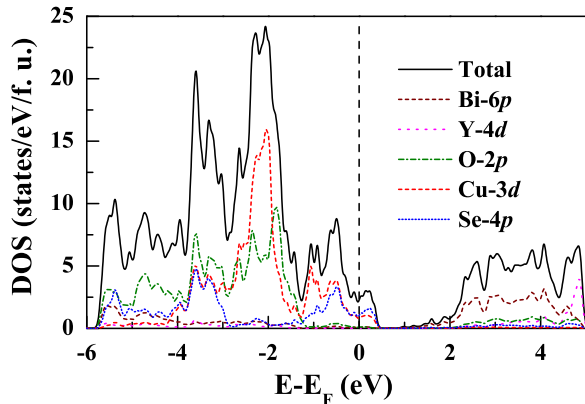


FIG. 8: The calculated DOS of $\text{Bi}_2\text{YO}_4\text{Cu}_2\text{Se}_2$.

materials such as MgB_2 ⁴⁵ as well as in iron based material $\text{Nd}(\text{O},\text{F})\text{FeAs}$ ⁴⁶. A multiband electronic structure at the Fermi level is also supported by the DFT calculations discussed below.

C. Electronic Structure of $\text{Bi}_2\text{YO}_4\text{Cu}_2\text{Se}_2$.

The crystal structure of $\text{Bi}_2\text{YO}_4\text{Cu}_2\text{Se}_2$ was optimized with respect to lattice parameters and atomic positions. The optimized lattice parameters and atomic coordinates are listed in Table IV. The structure is in good agreement with experimental observation except for the slight overestimation of c -axial lattice parameter ($(c_{\text{opt.}} - c_{\text{exp.}})/c_{\text{exp.}} = 2.3\%$), which is expected within the GGA calculation. Nonmagnetic (NM), ferromagnetic (FM), checkerboard and stripes antiferromagnetic (AFM) states are tested in the system. The magnetic moments of each atom in FM and AFM states are converged to zero, which is consistent with the magnetic properties measured in experiment.

Figure 8 shows the calculated DOS of $\text{Bi}_2\text{YO}_4\text{Cu}_2\text{Se}_2$. The finite DOS at Fermi level (E_F) indicates the metallic ground state, consistent with the experimental results. In the valence band, Bi-6*p* electrons hybridize with O-2*p* electrons in the energy range between -6 eV and -1 eV, and the hybridization of Cu-3*d* and Se-4*p* electrons is from -6 eV to 0.5 eV across E_F . The conduction

bands at higher energy, mainly built up of Bi-6*p* and O-2*p* electrons, are separated by a small gap of 0.25 eV. The E_F locates at a small valley of DOS, leading to the small $N(E_F)$. The calculated $N(E_F)$ (2.1 states/eV/f. u.) is slightly larger than the experimental one (1.5 states/eV/f. u.), which may be due to existence of the small amount of Se deficiency in our polycrystalline sample and the semiconducting impurity BiOCuSe .

Figure 9(a) shows the band structure of $\text{Bi}_2\text{YO}_4\text{Cu}_2\text{Se}_2$. In the Γ -Z direction (perpendicular to the layers), the bands are rarely dispersive. On the other hand, the strong hybridizations between Cu and Se give rise to a strongly dispersive band structure in the layer-parallel directions. Similar quasi-2D properties are found in alkali metal intercalated compound KCu_2Se_2 , which also behaves metallic.²⁰ There are two bands crossing E_F . For the lower one (line in blue in Fig. 9(a)), there are two hole cylinders: One locates at zone center, and another locates around Σ and Σ_1 points. The large electron cylinder around the zone corner is from the upper band crossing E_F (line in red in Fig. 9(a)). The total volume outside the electron cylinders and the volume confined in the hole cylinders contain one hole/f. u..

In order to interpret the temperature dependence of hall coefficient qualitatively, the simple two-band model was introduced^{46,47}:

$$R_H = \frac{\sigma_1^2 R_1 + \sigma_2^2 R_2}{(\sigma_1 + \sigma_2)^2}, \quad (5)$$

where $R_i = 1/n_i q$ represents the Hall coefficient for the carriers in each band separately with n_i the concentration of the charge carriers in the different bands. σ_i ($i = 1, 2$) is the conductance of the charge carriers in different bands, which can be expressed as $\sigma_i = \frac{|q|^2 \tau_i n_i}{m_i^*}$, where the m_i^* is the effective mass, and τ_i is the relaxation time in each band. Normally, the carrier concentration rarely varies with the temperature. Since the multiple Fermi pockets locate at different position with different shape in $\text{Bi}_2\text{YO}_4\text{Cu}_2\text{Se}_2$, it is natural that they have different effective mass and Fermi velocity of them. The scattering should also share the low similarities. Therefore, the carriers in different bands may have different τ_i , which varies differently with temperature. Each band can produce complex contributions to the total R_H , which lead to the variation of R_H with temperature.

In order to analyze the orbital characters, the ‘‘fat-band’’ of $\text{Bi}_2\text{YO}_4\text{Cu}_2\text{Se}_2$ is also presented (Fig. 10). Obviously, the Fermi surface is formed by the bands with prominent hybridization between $d_{xy} + d_{yz}$ of Cu and $p_x + p_y$ of Se. The Se- p_z orbital has almost no contribution at E_F , indicating the absence of conduction between the layers. Such quasi-2D electronic properties of $\text{Bi}_2\text{YO}_4\text{Cu}_2\text{Se}_2$ needs to be further confirmed by experimental studies on the single crystal.

We also performed a GGA+ U calculation for NM, FM, checkerboard AFM, and stripes AFM states considering the strong Coulomb correlation of 3*d* electrons in

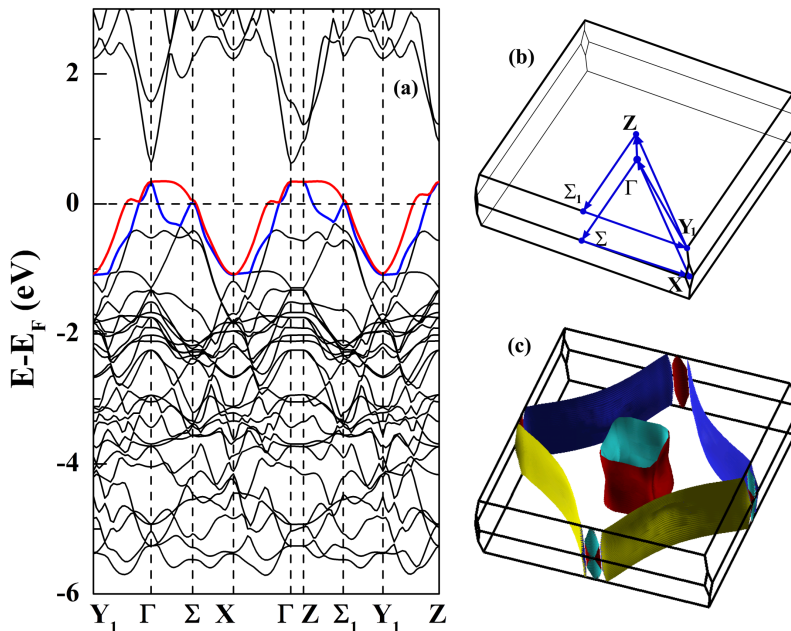


FIG. 9: (a) The band structure, (b) The Brillouin zone and (c) Fermi surface of $\text{Bi}_2\text{YO}_4\text{Cu}_2\text{Se}_2$. The red and blue lines in (a) denote the bands crossing E_F . The high symmetry points are denoted in (b).

$\text{Bi}_2\text{YO}_4\text{Cu}_2\text{Se}_2$. The magnetic moments of each atom in FM and AFM states are converged to zero as well. The corresponding DOS of NM state are presented in Fig. 11. It can be found that the Coulomb interactions moves the weight of $3d$ electrons towards lower energy. Such properties have been reported in some NiSe-based superconductors.⁴⁸ Under different U , the $d_{xy} + d_{yz}$ orbitals remain contributing prominently at E_F , which makes the $N(E_F)$ rarely varies. Unquestionably, the added Coulomb interactions do not make the system become a Mott insulator. It might be because of the $3d^{9.5}$ configuration of Cu in $\text{Bi}_2\text{YO}_4\text{Cu}_2\text{Se}_2$, for which the five orbitals of Cu- $3d$ are almost full filled.⁴⁸

D. Ground States of $\text{Bi}_2\text{YO}_4\text{Cu}_2\text{Se}_2$ -type Compounds: A DFT Analysis

Based on the calculation above, the metallic ground state of $\text{Bi}_2\text{YO}_4\text{Cu}_2\text{Se}_2$ is verified. However, to the best of our knowledge, most undoped $\text{CuCh}(\text{Ch}=\text{S}, \text{Se})$ -based compounds are semiconductors (see Table I). The origin of metallic ground states of $\text{Bi}_2\text{YO}_4\text{Cu}_2\text{Se}_2$ -type compounds need to be distinctly clarified. Generally speaking, CuSe-based compounds can be seen as Cu_2Se_2 layer intercalated by some atoms or molecules. Since the valence band maximum (VBM) is mainly composed of the Cu-Se hybridization states, the function of intercalated blocking layers can be simply seen as giving their valence electrons to the bands. All the reported CuSe-based semiconductors have the bivalent blocking layers, in which Cu- $3d$ bands are full filled. When the valence of the blocking layer is smaller than +2, the Cu- $3d$

bands are partly occupied, leading to the metallic ground state (e.g. $[\text{HgO}]^0 + \text{CuSe}^{25}$ and $\text{K}^1 + \text{Cu}_2\text{Se}_2^{20}$). Figure 12 shows the DOS of BiOCuSe , LaOCuSe , $\text{Bi}_2\text{YO}_4\text{Cu}_2\text{Se}_2$, and hypothetical $\text{La}_3\text{O}_4\text{Cu}_2\text{Se}_2$. For the semiconducting BiOCuSe and LaOCuSe , the $\text{Bi}_2\text{O}_2/\text{La}_2\text{O}_2$ blocking layers are bivalent. According to the XPS measurements mentioned above, Bi_2YO_4 layer only gives one valence electron. Similarly, the La_3O_4 layer should be monovalent. In that case, there is one hole in the valence band, making the systems become metals with p -type carriers. Such trend is consistent with the case of ACu_2Se_2 (A is alkali or alkali earth metal).²⁰

If this trend is universal for all the CuSe-based compounds, one may expect that the one electron doping will make $\text{Bi}_2\text{YO}_4\text{Cu}_2\text{Se}_2/\text{La}_3\text{O}_4\text{Cu}_2\text{Se}_2$ semiconducting. We calculated the DOS under such doping of $\text{Bi}_2\text{YO}_4\text{Cu}_2\text{Se}_2$ and $\text{La}_3\text{O}_4\text{Cu}_2\text{Se}_2$ using the rigid band approximation (RBA) (Fig. 13 (a) and (b)). The results show that the electron doping raises E_F to the VBM. In reality, such doping needs to be processed by replacing the trivalent cation Bi/Y/La with a tetravalent cation, or replacing the bivalent anion O with monovalent anions. So we calculated the DOS of $\text{Bi}_2\text{YO}_4\text{Cu}_2\text{Se}_2$ and $\text{La}_3\text{O}_4\text{Cu}_2\text{Se}_2$ with the substitution of the typical tetravalent cations Zr and Sn, and monovalent anion F. The optimized structural parameters of these doped samples are presented in Table V. Figures 13 (c)-(h) show the calculated DOS of these samples. The E_F is indeed moved to the top of Cu- $3d$ bands by the substitutions. For $\text{Bi}_2\text{ZrO}_4\text{Cu}_2\text{Se}_2$, $\text{La}_2\text{ZrO}_4\text{Cu}_2\text{Se}_2$, and $\text{La}_3\text{O}_3\text{FCu}_2\text{Se}_2$, the semiconducting ground states are obtained as expected. Surprisingly, for the Sn-doped samples, the bands of Sn- $5s$ oc-

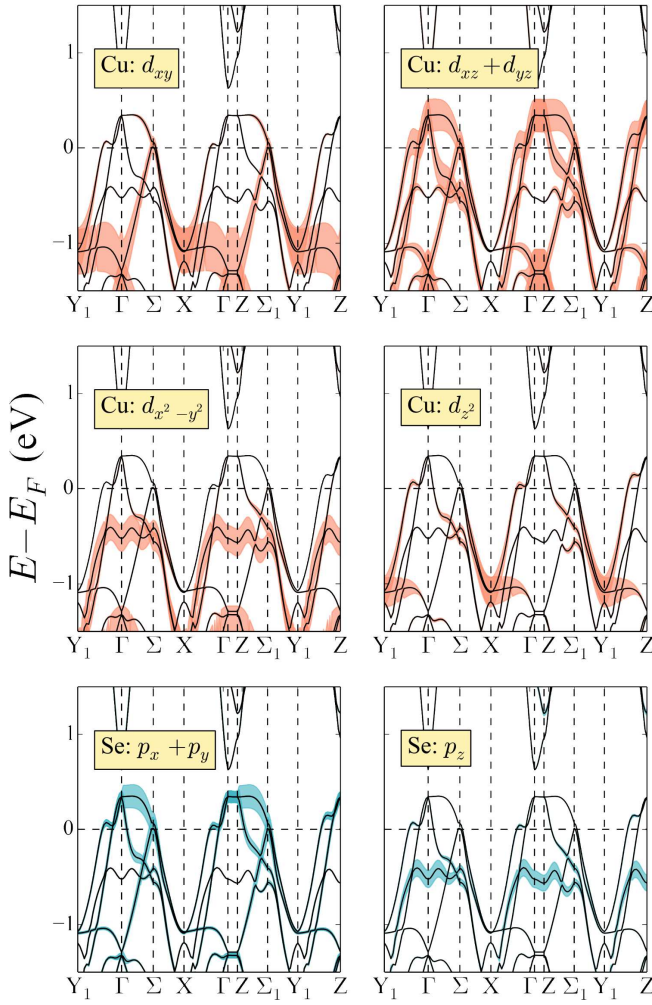


FIG. 10: “Fat bands” of $\text{Bi}_2\text{YO}_4\text{Cu}_2\text{Se}_2$, decorated with partial orbital characters of Cu and Se.

cur at E_F , leading to the metallic ground state. For $\text{Bi}_2\text{YO}_3\text{FCu}_2\text{Se}_2$, the hybridizations between Bi and F move the conduction band downwards, and as a result, a pseudogap was obtained. Obviously, when the Cu- $3d$ bands are fully occupied, the bands of the blocking layer determine the ground states for these samples.

In fact, the Bi_2YO_4 -type layer can be seen as a stacking of two Bi_2O_2 -type slabs. If we insert more Bi_2O_2 -type slabs into the compounds, we can get a series of compounds with the general formula $[\text{A}_2\text{X}_2(\text{AX}_2)_n]\text{Cu}_2\text{Se}_2$ (A is metal cation, X is anion). One can always choose the appropriate atoms to construct the $[\text{A}_2\text{X}_2(\text{AX}_2)_n]$ -type blocking layer by forcing the $[\text{A}_2\text{X}_2(\text{AX}_2)_n]$ to behave an expected valence. Figure 14 show the semiconducting examples of $[\text{Sr}_2\text{F}_2(\text{SrF}_2)_n]\text{Cu}_2\text{Se}_2$ with $n = 0$ and 1. The $[\text{Sr}_2\text{F}_2(\text{SrF}_2)_n]$ -type blocking layer is bivalent no matter how many the Sr_2F_2 -type slabs are introduced.

In the $[\text{A}_2\text{X}_2(\text{AX}_2)_n]\text{Cu}_2\text{Se}_2$ -type compounds, the conduction band minimum (CBM) of such compounds are composed of the bands of cation A. When the anion $\text{X} = \text{O}$, in order to have a bivalent blocking layer, the

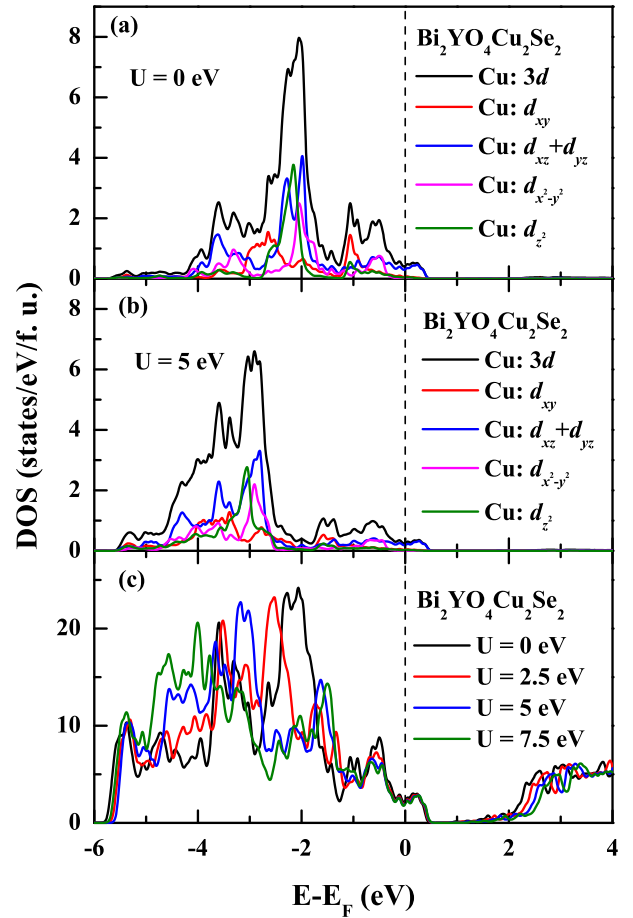


FIG. 11: (a) Orbital contribution of DOS of Cu- $3d$ electrons with $U = 0$ eV. (b) Orbital contribution of DOS of Cu- $3d$ electrons with $U = 5$ eV. (c) DOS of $\text{Bi}_2\text{YO}_4\text{Cu}_2\text{Se}_2$ with $U = 0, 2.5, 5,$ and 7.5 eV.

TABLE V: The optimized lattice parameters of some hypothetical compounds.

| | a(Å) | b(Å) | c(Å) |
|---|-------|-------|--------|
| $\text{Bi}_2\text{ZrO}_4\text{Cu}_2\text{Se}_2$ | 3.792 | 3.792 | 23.983 |
| $\text{Bi}_2\text{SnO}_4\text{Cu}_2\text{Se}_2$ | 3.832 | 3.832 | 23.978 |
| $\text{Bi}_2\text{YO}_3\text{FCu}_2\text{Se}_2$ | 3.845 | 3.953 | 23.998 |
| $\text{La}_3\text{O}_4\text{Cu}_2\text{Se}_2$ | 4.091 | 4.091 | 24.258 |
| $\text{La}_2\text{ZrO}_4\text{Cu}_2\text{Se}_2$ | 3.897 | 3.897 | 23.577 |
| $\text{La}_2\text{SnO}_4\text{Cu}_2\text{Se}_2$ | 3.938 | 3.938 | 23.409 |
| $\text{La}_3\text{O}_3\text{FCu}_2\text{Se}_2$ | 4.030 | 4.115 | 23.570 |
| SrFCuSe | 4.084 | 4.084 | 8.881 |
| $\text{Sr}_3\text{F}_4\text{Cu}_2\text{Se}_2$ | 4.073 | 4.073 | 23.752 |

valence of the cation A must be greater than or equal to +3. Some A with high valence state can lead to very deep CBM. For example, the deep CBM of Bi^{2+} leads to the small gap of $\text{Bi}_2\text{ZrO}_4\text{Cu}_2\text{Se}_2$ and the pseudogap of $\text{Bi}_2\text{YO}_3\text{FCu}_2\text{Se}_2$. The deeper CBM of Sn is overlapped with VBM, leading to the metallic ground

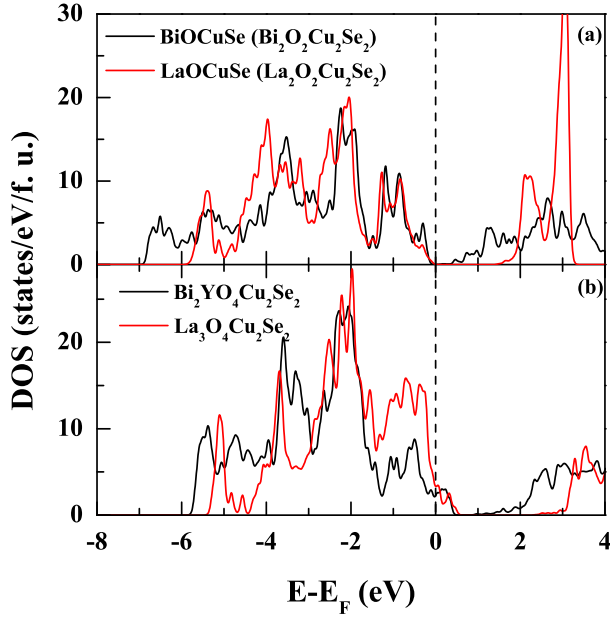


FIG. 12: (a) The DOS of BiOCuSe and LaOCuSe. (b) The DOS of Bi₂YO₄Cu₂Se₂, and a hypothetical La₃O₄Cu₂Se₂.

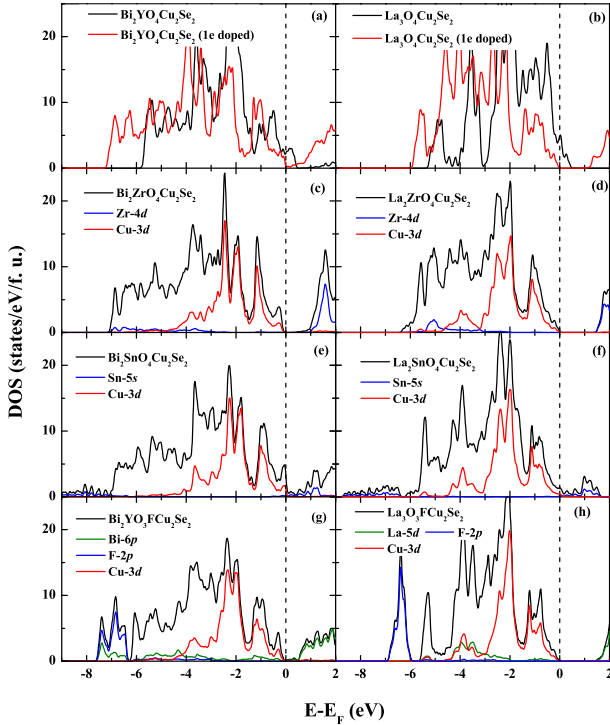


FIG. 13: The DOS of one electron doped in Bi₂YO₄Cu₂Se₂ (left panel) and La₃O₄Cu₂Se₂ (right panel). (a) and (b) show the doping effect simulated by simply adding an electron to the system based on RBA. (c)-(h) show the doping effect simulated by doping typical tetravalent cations Zr and Sn or a typical monovalent anion F.

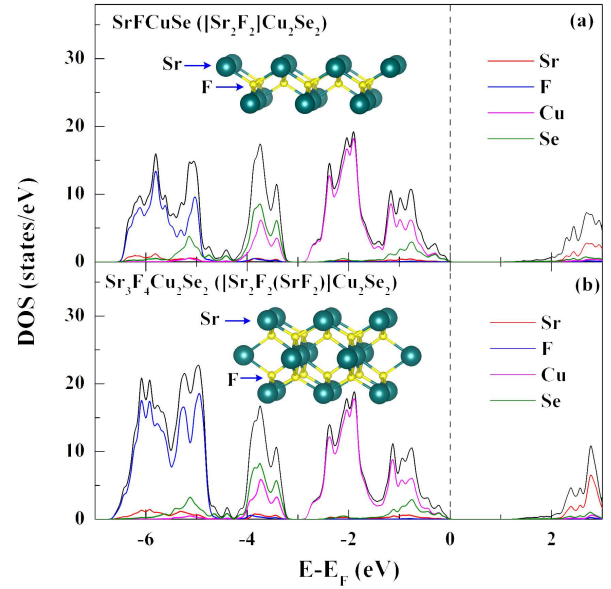


FIG. 14: The DOS of [Sr₂F₂(SF₂)_n]Cu₂Se₂ with (a) $n=0$ and (b) $n=1$. The insets show the structures of the [Sr₂F₂(SF₂)_n]-type blocking layers.

states of Bi₂SnO₄Cu₂Se₂ and La₂SnO₄Cu₂Se₂. Therefore, the ground state of [A₂X₂(AX₂)_n]Cu₂Se₂-type compounds can be tuned by designing the blocking layers. The small/large gap semiconductors and metals can be obtained for different applications.

IV. CONCLUSION

In summary, we systematically studied the physical properties of layered oxychalcogenide Bi₂YO₄Cu₂Se₂. It crystallizes in an unusual intergrowth structure with Cu₂Se₂ and Bi₂YO₄ layers. Bi₂YO₄Cu₂Se₂ exhibits metallic behavior with *p*-type carriers between 2 and 300 K. We obtained a rather large value of *ZT* at room temperature. Theoretical calculation confirms the quasi-2D metallic behavior of Bi₂YO₄Cu₂Se₂ and indicates the state at Fermi energy originates mainly from Cu-3*d* and Se-4*p* electrons.

Based on the comparison of the transport properties of the reported CuSe-based layered compounds, we found that the ground states of the known CuSe-based compounds are related to the valence electrons of their blocking layer: When the number of transferred valence electrons from blocking layer to Cu₂Se₂ layer is smaller than two per layer, the compounds would exhibit metallic behaviors (e.g. KCu₂Se₂²⁰, HgOCuSe²⁵), but if that number is two, they would become semiconductors. (e.g. BiOCuSe²²). However, according to our calculations, some Bi₂YO₄Cu₂Se₂-type compounds may not obey the rules. The theoretical investigation of doping effects in the system indicates that the ground states of the Bi₂YO₄Cu₂Se₂-type compounds can be tuned by design-

ing the blocking layers. The small/large gap semiconductors and metals can be obtained for different applications. The physical properties of other CuSe-based layered compounds need to be studied in the future in order to examine our deduction.

Note: In the first version, we mistyped the lattice parameters for some sample when calculating the doping effects of $\text{Bi}_2\text{YO}_4\text{Cu}_2\text{Se}_2$ and $\text{La}_3\text{O}_4\text{Cu}_2\text{Se}_2$, which influence the obtained ground states, but will not change the discussions of the properties of $\text{Bi}_2\text{YO}_4\text{Cu}_2\text{Se}_2$. The errors have been corrected in this version. We are sorry for such confusions.

Acknowledgments

This work was supported by the National Key Basic Research under contract No. 2011CBA00111, and the

National Nature Science Foundation of China under contract Nos. 51102240, 11104279 and the Joint Funds of the National Nature Science Foundation of China and the Chinese Academy of Sciences Large-scale Scientific Facility (Grant No.U1232139) and Director's Fund of Hefei Institutes of Physical Science, Chinese Academy of Sciences. The calculations were partially performed at the Center for Computational Science, CASHIPS.

* The authors contributed equally to this work.

† Corresponding author: hchlei@issp.ac.cn

‡ Corresponding author: ypsun@issp.ac.cn

¹ W. K. Wong-ng, K. L. Davis, and R. S. Roth, *J. Am. Ceram. Soc.* **71**, C64 (1988).

² T. Kimura, and Y. Tokura, *Annu. Rev. Mater. Sci.* **30**, 451 (2000).

³ A. Maignan, S. Hebert, L. Pi, D. Pelloquin, C. Martin, C. Michel, M. Hervieu, and B. Raveau, *Cryst. Eng.* **5**, 365 (2002).

⁴ S. J. Clarke, P. Adamson, S. J. C. Herkelrath, O. J. Rutt, D. R. Parker, M. J. Pitcher, and C. F. Smura, *Inorg. Chem.* **47**, 8473 (2008).

⁵ Y. Kamihara, T. Watanabe, M. Hirano, and H. Hosono, *J. Am. Chem. Soc.* **130**, 3296 (2008).

⁶ Y. Kamihara, H. Hiramatsu, M. Hirano, R. Kawamura, H. Yanagi, T. Kamiya, and H. Hosono, *J. Am. Chem. Soc.* **128**, 10012 (2006).

⁷ M. Palazzi, *Acad. Sci., Paris, C. R.* **292**, 789 (1981).

⁸ M. Palazzi, C. Carcaly, and J. Flahaut, *J. Solid State Chem.* **35**, 150 (1980).

⁹ K. Ueda, S. Inoue, S. Hirose, H. Kawazoe, and H. Hosono, *Appl. Phys. Lett.* **77**, 2701 (2000).

¹⁰ H. Hiramatsu, H. Kamioka, K. Ueda, M. Hirano, and H. Hosono, *J. Ceram. Soc. Jpn.* **113**, 10 (2005).

¹¹ E. Brechtel, G. Cordier, and H. Schaefer, *Z. Naturforsch., B: Anorg. Chem., Org. Chem.* **34**, 777 (1979).

¹² M. Enjalran, R. T. Scalettar, and S. M. Kauzlarich, *Phys. Rev. B* **61**, 14570 (2000).

¹³ T. C. Ozawa, S. M. Kauzlarich, M. Bieringer, C. R. Wiebe, J. E. Greedan, and J. S. Gardner, *Chem. Mater.* **13**, 973 (2001).

¹⁴ W. J. Zhu, and P. H. Hor, *J. Solid State Chem.* **130**, 319 (1997).

¹⁵ W. J. Zhu, P. H. Hor, A. J. Jacobson, G. Crisci, T. A. Albright, S. -H. Wang, and T. Vogt, *J. Am. Chem. Soc.* **119**, 12398 (1997).

¹⁶ K. Otzsch, H. Origino, J. Shimoyama, and K. Kishio, *J. Low Temp. Phys.* **117**, 729 (1999).

¹⁷ P. Adamson, J. Hadermann, C. F. Smura, O. J. Rutt, G.

Hyett, D. G. Free, and S. J. Clarke, *Chem. Mater.* **24**, 2802 (2012).

¹⁸ C. F. Smura, D. R. Parker, M. Zbiri, M. R. Johnson, Z. A. Gál, and S. J. Clarke, *J. Am. Chem. Soc.* **133**, 2691 (2011).

¹⁹ S. F. Jin, X. L. Chen, J. G. Guo, M. Lei, J. J. Lin, J. G. Xi, W. J. Wang, and W. Y. Wang, *Inorg. Chem.* **51**, 10185 (2012).

²⁰ O. Tiedje, E. E. Krasovskii, W. Schattke, P. Stoll, C. Näther, and W. Bensch *Phys. Rev. B* **67**, 134105 (2003).

²¹ A. Krishnapriyan, P. T. Barton, M. Miao, and R. Seshadri, [arXiv: 1309.3041v1](https://arxiv.org/abs/1309.3041v1).

²² H. Hiramatsu, H. Yanagi, T. Kamiya, K. Ueda, M. Hirano, and H. Hosono, *Chem. Mater.* **20**, 326 (2008).

²³ H. Yanagi, J. Tate, S. Park, C. -H. Park, D. A. Keszler, M. Hirano, and H. Hosono, *J. Appl. Phys.* **100**, 083705 (2006).

²⁴ K. Ueda, K. Takafuji, H. Yanagi, T. Kamiya, H. Hosono, H. Hiramatsu, M. Hirano, and N. Hamada, *J. Appl. Phys.* **102**, 113714 (2007).

²⁵ G. C. Kim, M. Cheon, I. S. Park, D. Ahmad, and Y. C. Kim, [arXiv:1105.5868v1](https://arxiv.org/abs/1105.5868v1).

²⁶ M. -L. Liu,; L. -B. Wu,; F. -Q. Huang,; L. -D. Chen, I. -W. Chen, *J. Appl. Phys.* **102**, 116108 (2007).

²⁷ D. O. Scanlon, and G. W. Watson, *Chem. Mater.* **21**, 5435 (2009).

²⁸ G. V. Vajenine, and R. Hoffmann, *Inorg. Chem.* **35**, 451 (1996).

²⁹ Y. Takano, K. Yahagi, and K. Sekizawa, *Physica B* **206**, 764 (1995).

³⁰ K. Ueda, S. Hirose, H. Kawazoe, and H. Hosono, *Chem. Mater.* **13**, 1880 (2001).

³¹ J. S. O. Evans, E. B. Brogden, A. L. Thompson, and R. L. Cordiner, *Chem. Commun.* 912 (2002).

³² B. Hunter, *Int. Un. of Cryst. Comm. Newsletter* **20** (1998).

³³ J. P. Perdew, K. Burke, and M. Ernzerhof, *Phys. Rev. Lett.* **77**, 3865 (1996).

³⁴ P. Giannozzi, *et al.* *J. Phys.: Condens. Matter* **21**, 395502 (2009).

³⁵ K. F. Garrity, J. W. Bennett, K. M. Rabe, and D. Vander-

- bilt, *Comput. Mater. Sci.* **81**, 446 (2014).
- ³⁶ V. I. Anisimov, I. V. Solovyev, M. A. Korotin, M. T. Czyżyk, and G. A. Sawatzky, *Phys. Rev. B* **48**, 16929 (1993).
- ³⁷ A. I. Liechtenstein, V. I. Anisimov, and J. Zaanen, *Phys. Rev. B* **52**, R5467 (1995).
- ³⁸ H. J. Monkhorst, and J. D. Pack, *Phys. Rev. B* **13**, 5188 (1976).
- ³⁹ T. P. Debies, and J. W. Rabalais, *Chem. Phys.* **20**, 277 (1977).
- ⁴⁰ R. P. Vasquez, M. C. Foote, and B. D. Hunt, *J. Appl. Phys* **66**, 4867 (1989).
- ⁴¹ J. Haber, T. Machej, L. Ungier, and J. Ziolkowski, *J. Solid State Chem.* **25**, 207 (1978).
- ⁴² R. Romand, M. Roubin, and J. P. Deloume, *J. Electron Spectrosc. Relat. Phenom.* **13**, 229 (1978).
- ⁴³ J. Svorec, M. Valko, J. Mondol, M. Mazúr, M. Melník, and J. Telsler, *Transition Met. Chem.* **34**, 129 (2009).
- ⁴⁴ C. Barreateau, D. Bèardan, E. Amzallag, L. D. Zhao, and N. Dragoe, *Chem. Mater.* **24**, 3168 (2012).
- ⁴⁵ H. Yang, Y. Liu, C. Zhuang, J. Shi, Y. Yao, S. Massidda, M. Monni, Y. Jia, X. Xi, Q. Li, Z. -K. Liu, Q. Feng, H. -H. Wen, *Phys. Rev. Lett.* **101**, 067001 (2008).
- ⁴⁶ P. Cheng, H. Yang, Y. Jia, L. Fang, X. Zhu, G. Mu, and H. H. Wen, *Phys. Rev. B* **78**, 134508 (2008).
- ⁴⁷ G. Mu, H. Yang, and H. H. Wen, *Phys. Rev. B* **82**, 052501 (2010).
- ⁴⁸ F. Lu, J. Z. Zhao, and W. H. Wang, *J. Phys.: Condens. Matter* **24**, , 495501 (2012).